Asian Journal of Basic Science & Research
Volume 8, Issue 2, Pages 15-28, April-June 2026

Identification of the Hydrocarbon Trapping Mechanisms in Onshore Fuba Field, Niger Delta, Nigeria Using Well Log and 3-D Seismic Data

U. Ochoma[1*]

[1]*Department of Physics, Rivers State University, P.M.B 5080, Port Harcourt, Nigeria.*
Corresponding Author (U. Ochoma) Email: umaocho@gmail.com[*]

DOI: Under Assignment

Copyright © 2026 U. Ochoma. This is an open-access article distributed under the terms of the Creative Commons Attribution License, which permits unrestricted use, distribution, and reproduction in any medium, provided the original author and source are credited.

Article Received: 19 February 2026 *Article Accepted: 22 April 2026* *Article Published: 24 April 2026*

ABSTRACT

Identification of the hydrocarbon trapping mechanisms in Onshore Fuba Field, Niger Delta, Nigeria using well log and 3D seismic data are here presented. Seismic interpretation was carried out using Petrel software. The structural interpretation of seismic data reveal highly synthetic and antithetic faults which are in line with faults trends identified in the Niger Delta. Of the 36 interpreted faults, only synthetic and antithetic faults are regional, running from the top to bottom across the field. These faults play significant roles in trap formation at the upper, middle and lower sections of the field. Two distinct horizons were mapped. Fault and horizon interpretation reveal closures which are collapsed crestal structures bounded by these two major faults. The depth structure maps reveal anticlinal faults. Reservoirs are found at a shallower depth from 10937 to 10997 ft and at a deeper depth ranging from 11681 to 11871 ft. The synthetic and antithetic faults act as good traps for the hydrocarbon accumulation in the study area. The variance values range from 0.0 to 1.0. The Variance edge analysis was used to delineate the prominent and subtle faults in the area. The RMS (root mean square) amplitude values range from 0 to 13,000 in reservoir M and from 0 to 9,000 in horizon O. The high values of RMS amplitudes in the maps are interpreted as high porosity lithologies, which are potential high quality hydrocarbon reservoirs. The results of spectral decomposition indicate the following: (a) areas of low frequency and high amplitude associated with known hydrocarbon zones. (b) The presence of small-scale faults, channels, lobes and angular unconformity in the field. The results from the study will help in the identification of hydrocarbon potentials of the field and also aid in making economic decisions.

Keywords: Hydrocarbon Zones; Growth Faults; Anticlinal; Spectral Decomposition; RMS Amplitude; Variance Method; Channels; Angular Unconformity; Niger Delta; Nigeria.

1. Introduction

3-D seismic interpretations are used to image subsurface structures capable of harbouring hydrocarbon (Richardson, and Taioli, 2018; Abimbola, and Emujakporue, 2020; Majid et al, 2016). Tectonic setting usually governs the structural network and associated features (Adebayo, et al, 2021). These traps may be structural, stratigraphic or a combination of both. Majority of traps in the Niger delta are structural (Coffen, 1984; Doust, E. Omatsola, 1990). Structural traps include the faults, anticlines and duplex (Emujakporue, and Ngwueke, 2013). Stratigraphic traps include sand channels, pinch-outs, unconformities and other truncations (Folami, et al, 2008). Detailed structural analysis will reveal the trapping mechanism of the oil field and this will help to avoid drilling of dry hole (Aigbedion, and Hafiz, 2016; Omoja, and Obiekezie, 2019).

This study is taken from Fuba Field, Depobelt, Niger Delta, Nigeria. The ultimate deliverable of this study was identification of the hydrocarbon trapping mechanisms of the area using well log and 3D seismic data. The major components of this study are: (a) Well Correlation performed in order to determine the continuity of the reservoir sand across the field. (b) Seismic Interpretation which involves well-to-seismic ties, fault mapping, horizon mapping, time surface generation, depth conversion and seismic attributes generation. This aids in giving more insight into identification of the hydrocarbon trapping mechanisms in Onshore Fuba Field, Niger Delta, Nigeria using well log and 3D seismic data.

The proposed study area Fuba Field is located in the onshore Niger Delta region. Figure 1 shows the map of the Niger Delta region showing the location of the study area and the base map showing well locations in the study area. The Niger Delta lies between latitudes 4° N and 6° N and longitudes 3° E and 9° E (Whiteman, 1982). The Delta ranks as one of the major oil and gas provinces globally, with an estimated ultimate recovery of 40 billion barrels of oil and 40 trillion cubic feet of gas (Adegoke et al., 2017). The coastal sedimentary basin of Nigeria has been the scene of three depositional cycles (Short and Stauble, 1967). The first began with a marine incursion in the middle Cretaceous and was terminated by a mild folding phase in Santonian time. The second included the growth of a proto-Niger delta during the Late Cretaceous and ended in a major Paleocene marine transgression. The third cycle, from Eocene to Recent, marked the continuous growth of the main Niger delta. A new threefold lithostratigraphic subdivision is introduced for the Niger delta subsurface, comprising an upper sandy Benin Formation, an intervening unit of alternating sandstone and shale named the Agbada Formation, and a lower shaly Akata Formation. These three units extend across the whole delta and each range in age from early Tertiary to Recent.

They are related to the present outcrops and environments of deposition. A separate member of the Benin Formation is recognized in the Port Harcourt area. It is Miocene-Recent in age with a minimum thickness of more than 6,000 ft (1829 m) and made up of continental sands and sandstones (>90 %) with few shale intercalations (Horsfall et al., 2017). Subsurface structures are described as resulting from movement under the influence of gravity and their distribution is related to growth stages of the delta (Ochoma, 2023). Rollover anticlines in front of growth faults form the main objectives of oil exploration, the hydrocarbons being found in sandstone reservoirs of the Agbada Formation. The oil in geological structures in the basin may be trapped in dip closures or against a synthetic or antithetic fault.

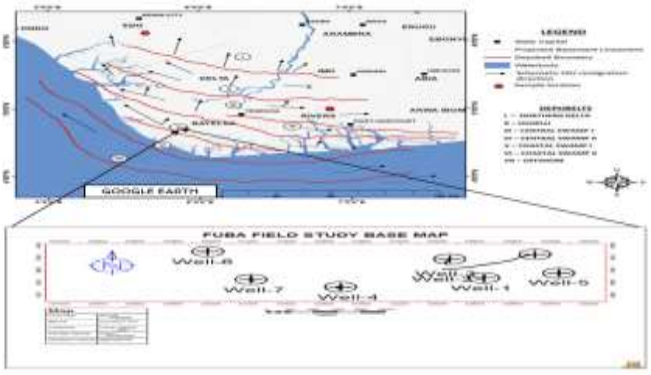

Figure 1. Map of Niger Delta Showing the Study Area

(Source: Google Earth 2026) and Base Map Showing Well Locations in the Study Area

1.1. Study Objectives

The objectives of the study include the following:

1) Mapping of faults.

2) Delineation of reservoir units.

3) Generation of synthetic seismogram and well-to-seismic tie.

4) Generation of time surfaces.

5) Generation of seismic attributes.

6) Converting reservoir surfaces from time to depth.

2. Literature

Several researchers have made enormous contributions based on structural interpretations and hydrocarbon trapping mechanisms within the Niger Delta basin to investigate the potentiality of hydrocarbon deposits (Ochoma, et al, 2023; Aizebeokhai, and Olayinka, 2011; Hafiz, et al, 2024; Ameloko, and Owoseni, 2015; Sulistiyono, et al, 2025; Yousif, et al, 2025). Hafiz, et al, 2024 well log petrophysical analysis revealed three reservoirs in onshore and three reservoirs in offshore which cut across four (4) wells respectively. Average reservoir parameters for the onshore such as porosity 30.01 % and hydrocarbon saturation 64.33 % with average thickness of 26.52 m while the offshore average reservoir parameters such as porosity 28.00 % and hydrocarbon saturation 77.67 % with average thickness of 10m were derived from petrophysical analysis. A total of three horizons and seven faults were mapped on the onshore seismic sections that indicated faulted anticlines, listric fault, growth fault, synthetic and antithetic fault were closely observed. While three horizons were mapped on the offshore seismic section that indicates back-to-back structures. The structural maps showed that the major structures accommodating the Hydrocarbon in both fields are fault assisted closure, four-way closures and growth faults. The trapping mechanisms were identified to be fault dependent. The RMS (root-mean-square) amplitude surface maps reveal sections with bright spot anomalies. The amplitude anomalies served as DHIs (direct hydrocarbon indicators). Seismic-to-well ties show the top of the Hydrocarbon bearing sand unit lie on top of the well on the seismic section in the field. While Ameloko, and Owoseni, (2015), in their study on hydrocarbon reservoir evaluation of X-field in the Niger Delta using seismic and petrophysical data, deduced from their results on structural interpretations that localized normal faults exist in the study area.

Sulistiyono, et al, (2025) in their study aimed to model the geological history and analyse structural controls on hydrocarbon trapping. The methods used are surface and subsurface geological structure analysis, including recording surface geological structures, fault fracture density analysis, identifying markers from well data, seismic interpretation, subsurface mapping, and making geological history models. Three tectonic phases influence the structural patterns in the Kendal Sub-basin. Beginning in the Early to Middle Miocene, rifting produced a half-graben. The Middle Miocene to Late Miocene north-south compression stage follows this. Finally, the Late Miocene to Late Pliocene fault stage as compression intensity increases, creates a thrust fold zone. The modelling of geological history is closely associated with the hydrocarbon trapping mechanism. Hydrocarbon generation occurs in the organic-rich Lower Cibulakan shale, with vertical migration through fault systems and lateral migration through rock pores until it is trapped in reservoir formations. This migration ceases once the hydrocarbon becomes trapped in the reservoir rock. The study identified two primary trap types: structural traps (e.g., thrust anticline, sub-thrust, horst block) and stratigraphic traps (e.g., pinch-out sand, built-up carbonate).

Yousif, et al, (2025) observed that in the Missan oilfields, the linkage among basement faults, halokinesis, and hydrocarbon accumulation, and their control on structural-trap geometry and seal effectiveness, remain

insufficiently constrained, especially the timing/drivers of salt piercing and its coupling with regional folding. To address this, they integrated 3D seismic, well-log, and surface data to quantify these interactions across adjacent fields. Results show a clear correspondence between surface topographic highs and subsurface salt-related deformation. Buzurgan exhibits limited fault reactivation with persistent folding until the Late Miocene, whereas Fauqi and Abu Ghirab record Pliocene reactivation and intense salt deformation that generate disharmonic syncline-over-anticline geometries. The listric–conjugate faults are structurally linked to deep-seated basement faults and display clear spatial alignment with their orientations, enhancing halokinesis and accommodating differential shortening. At the same time, hydrocarbon charge pathways are primarily governed by the intensity of deep-seated faulting and the effectiveness of salt sealing. Critically, the study integrates disparate geological processes—fault reactivation, salt tectonics, and hydrocarbon migration—into a single coherent, field-validated model for the region and provides a practical method to anticipate subsurface complexity. The results show that variations in fault intensity across three adjacent fields (Buzurgan, Fauqi, Abu Ghirab) correspond to distinct reservoir outcomes: minimal faulting in Buzurgan confines charge to deeper Mishrif reservoirs; moderate faulting in Fauqi permits entrapment in Mishrif and Kirkuk; and intense faulting in Abu Ghirab facilitates vertical leakage to shallow Kirkuk. Collectively, the work moved beyond isolated case descriptions to provide a unified, exploitable frame work for predicting how basement-involved faulting and salt mobility jointly control deformation style and hydrocarbon distribution in foreland basins.

3. Methodology

3.1. Well-log and Seismic Data Quality Control

Well correlation involves lithologic description, picking top and base of sand-bodies, fluid discrimination and then linking these properties from one well to another based on similarity in trends. Correlation of reservoir sands was achieved using the top and base of reservoir sands picked. The correlation process was possible based on similarity in the behaviour of the gamma ray log. In the Niger Delta, the predominant lithologies are sands and shales. In order to discriminate between these two lithologies in the subsurface, the gamma ray log is used. After defining the lithologies, the resistivity log was used for discriminating the type of fluid occurring within the pores in the rocks.

There are six basic steps involved in seismic interpretation relevant to this study and they include well-to-seismic ties, Fault Mapping, Horizon mapping, Time surface generation, Depth Conversion and generation of seismic attributes. The sonic log, which is the reciprocal of velocity, was calibrated using the checkshot data. The calibration process is necessary in order to improve the quality of the sonic log because the sonic log is prone to washouts and other wellbore related issues. The results of calibrating the sonic log with the checkshot gives the calibrated sonic log.

The calibrated sonic log is used along with the density log to generate an acoustic impedance (AI) log. The acoustic impedance log is calculated for each layer of rock. The next step involves generating the RC (reflectivity coefficient) log. The RC is calculated and generated using the AI log. The RC log generated is then convolved with a wavelet to generate a synthetic seismogram which is comparable with the seismic data. The extended white 2 wavelet utilized for convolution is extracted from the seismic data. The synthetic seismogram was generated. The mathematical expressions that govern the entire well-to-seismic tie workflow are presented below:

$$AI = \rho v \quad (1)$$

$$RC = \frac{\rho_2 v_2 - \rho_1 v_1}{\rho_2 v_2 + \rho_1 v_1} \quad (2)$$

$$\text{Synthetic Seismogram} = \frac{\rho_2 v_2 - \rho_1 v_1}{\rho_2 v_2 + \rho_1 v_1} * wavelet \quad (3)$$

where AI = acoustic impedance, RC = reflection coefficient, ρ = density; v = velocity.

Faults were identified as discontinuities or breaks in the seismic reflections. Faults were mapped on both inline and cross-line directions. Horizons are continuous lateral reflection events that are truncated by fault lines. The horizon interpretation process was conducted along both inline and crossline direction. At the end of the horizon mapping, a seed grid is generated which serves as an input for time surface generation. Time surfaces were generated using the seed grids gotten from the horizon mapping process. The third order polynomial velocity model was generated and used to depth convert the time surfaces of the reservoirs of interest.

3.2. Variance (Edge Detection) Method

The variance attribute is edge imaging and detection techniques. It is used for imaging discontinuity related to faulting or stratigraphy in seismic data. Variance attribute is proven to help in imaging of channels, fault zones, fractures, unconformities and the major sequence boundaries (Pigott. et al, 2013). In the Petrel software, the variance attribute uses an algorithm that computes the local variance of the seismic data through a multi-trace window with user-defined size. The local variance is computed from horizontal sub-slices for each voxel. A vertical window was used for smoothing the computed variance and the observed amplitude normalized. The variance attribute measures the horizontal continuity of the amplitude that is the amplitude difference of the individual traces from their mean value within a gliding CMP window.

$$\sigma^2 = \frac{1}{n}\sum_{f_i=1}^{n}(x_i + x_m)^2 \quad (4)$$

Where σ = standard deviation, σ^2 = variance, n = the number of observations, f_i = frequency

x_i = the variable, x_m = mean of x_i.

3.3. Determination of RMS (Root Mean Square) Amplitude

The root mean square (RMS) amplitude was extracted from the seismic data as a surface attribute. Root mean square (RMS) amplitude is used to obtain a scaled estimate of seismic trace envelope. It is obtained in the software by sliding a tapered window of N samples as the square root of the sum of all the trace value x squared. The RMS attribute computation in Petrel software makes use of the inbuilt formula:

$$X_{rms} = \sqrt{\frac{1}{N}\sum_{n=1}^{N} w_n x_n^2} \quad (5)$$

where X_{rms} = root mean square amplitude, w_n = window values, N = number of samples in the window, x = trace value.

3.4. Spectral Decomposition

Spectral decomposition is a frequency attribute. It involves separating and classifying seismic events within each trace based on their frequency content. Each 1D trace was decomposed from the time domain into its corresponding 2D representation in the time-frequency domain using algorithms. Once each trace was transformed into the time-frequency domain, a band-pass filter was applied to view the amplitude of seismic data at different frequencies.

The short-time Fourier transform (STFT) spectrogram which is the squared modulus of the STFT and the spectral energy density is defined as (Cohen, 1989)

$$SP_s(t, f) = /\int_{-\infty}^{\infty} s(\tau)h(\tau - t)e^{-j2\pi f\tau}d\tau /^2 \qquad (6)$$

Where, $h(\tau - t)$ = the window function, $s(\tau)$ = the signal, SP_s = the short-time Fourier transform

j = the imaginary unit, τ = the time delay.

The relationships between the amplitude spectrum ($A(\omega)$) and the phase spectrum ($\gamma(\omega)$) of the estimated transformed signals are presented in equations 7 and 8

$$/A(\omega^T)/ = \sqrt{A_r + A_i} \qquad (7)$$

$$\gamma(\omega) = \mathrm{Tan}^{-1}[\frac{A_i}{A_r}] \qquad (8)$$

Where, A_r = real part of $A(\omega^T)$, A_i = imaginary part of $A(\omega^T)$, ω =frequency, T = transform of the signal, $A(\omega^T)$ = amplitude of transformed trace at frequency ω.

4. Results and Discussions

4.1. Reservoir Identification, Correlation and Well-to-Seismic Ties

The results for lithology and reservoir identification are presented in (Figure 2). A total of four sand bodies (L, M, N, O) were identified and correlated across all seven wells in the field. Two reservoir sands were selected for the purpose of this study (M and O). The resistivity logs which reveal the presence of hydrocarbons were used to identify the hydrocarbon bearing sands. On (Figure 2), the sands are coloured yellow while shales are grey in colour. The results for well-to-seismic tie conducted on Fuba field using density log, sonic log and check shot of Well-1 is presented in Figure 3. Extended white 2 wavelet was used to give a near perfect match between the seismic and synthetic seismogram.

4.2. Faults and Horizons Interpretation

The results for the interpreted faults in Fuba field are presented in Figure 4 shows both synthetic and antithetic faults interpreted along seismic in lines. Faults are more visible along the inline direction because this direction reveals

the true dip position of geologic structures. Figure 5 shows interpreted faults displayed on 3D interpretation window. The variance time slice at Z= 2060 was used to validate the interpreted faults as seen on Figure 6. All interpreted faults are normal synthetic and antithetic faults. A total of thirty-six faults were interpreted across the entire seismic data. Of the 36 interpreted faults, only F1 (synthetic fault) and F4 (antithetic fault) faults are regional, running from the top to bottom across the field. Hence, these faults play significant roles in trap formation at the upper, middle and lower sections of the field. The results for the interpreted seismic horizons (Horizon M and Horizon O) are also presented in Figure 4. On these horizons, the fault polygons were generated and eliminated. The horizons were used as inputs for the generation of reservoir time surfaces.

The reservoir time surfaces (M and O reservoirs) reveal that the reservoir structure is a collapsed crest, bounded by two regional faults (F1 and F4). Reservoir M and O time surfaces are truncated by two bounding faults and three minor inter-reservoir faults. The similarity in structure identified on reservoirs M and O reveal that the field is structurally controlled by faults. Figure 7 shows the 3rd order polynomial velocity model which was used as most suitable velocity model for converting M and O reservoirs from time to depth. The depth converted reservoir M and O reservoir surfaces are presented in Figures 8 and 9 for the third order polynomial velocity function. The depth structure maps reveal that the reservoirs are anticlinal and fault supported. Reservoir M is found at a shallower depth from 10937 to 10997 ft and at a deeper depth ranging from ft while reservoir O is found at a deeper depth ranging from 11681 to 11871 ft.

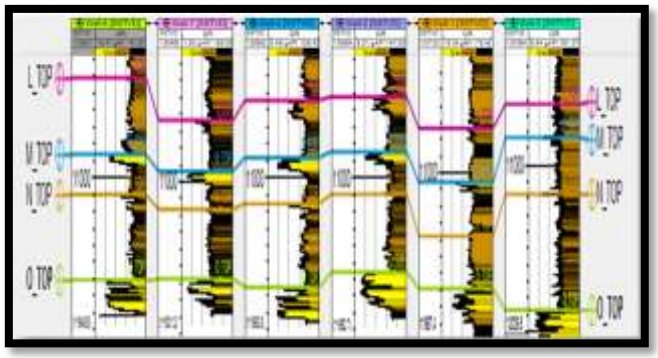

Figure 2. Well Section Showing Reservoirs L**,** M, N and O Identified and Correlated Across Fuba Field

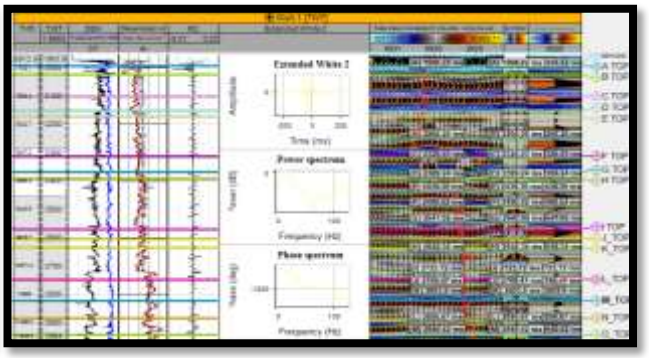

Figure 3. Synthetic Seismogram Generation and Well-to-seismic Tie Conducted for Fuba Field using Well-1 Checkshot

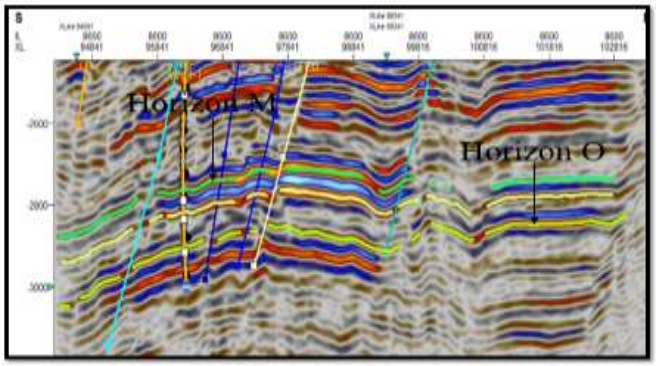

Figure 4. Faults (Synthetic and Antithetic) and Horizons M and O Interpreted Along Seismic Inline

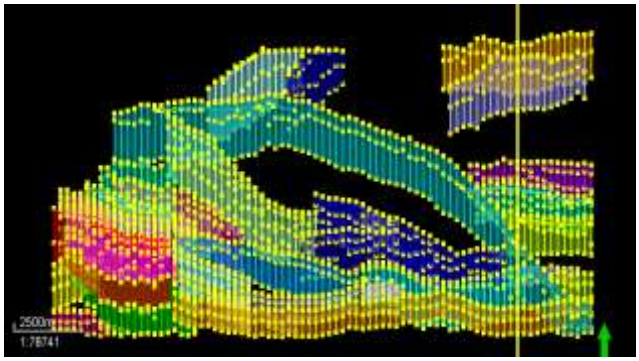

Figure 5. Interpreted Faults (Synthetic and Antithetic) Displayed on 3D Interpretation Window

Asian Journal of Basic Science & Research
Volume 8, Issue 2, Pages 15-28, April-June 2026

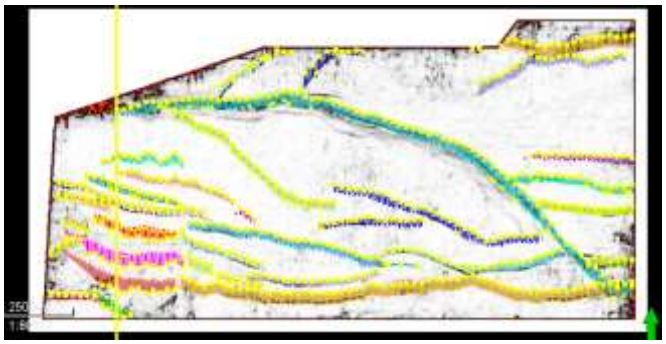

Figure 6. Interpreted Faults Displayed on the Variance Time Slice at Z=2060 used to Validate the Interpreted.

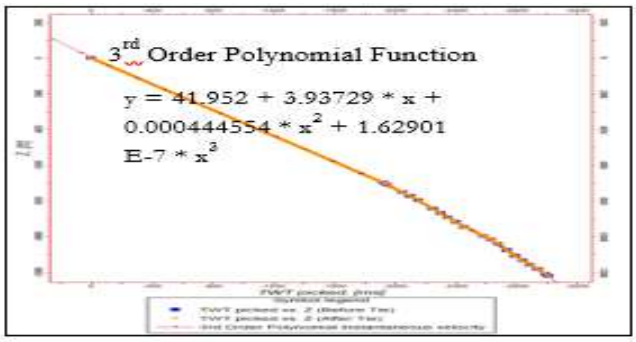

Figure 7. Third Order Polynomial Velocity Model Utilized for Converting Reservoir Surfaces M and O from Time to Depth

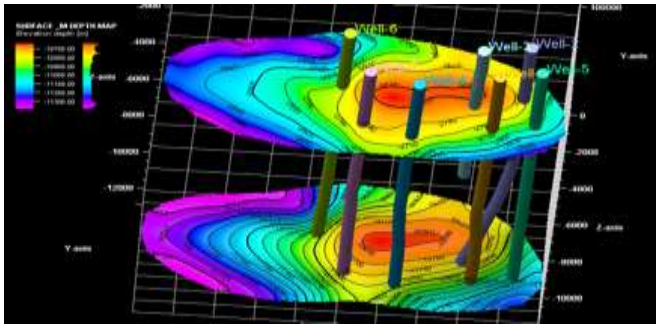

Figure 8. Reservoir Surface for Depth Surface M Indicating that reservoir M is Anticlinal and Fault Supported.

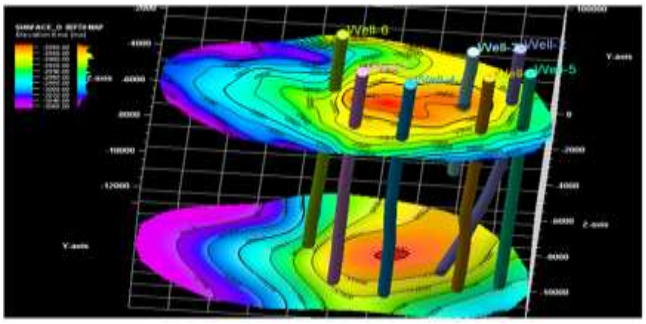

Figure 9. Reservoir Surface for Depth Surface O Indicating that Reservoir O is Anticlinal and Fault Supported

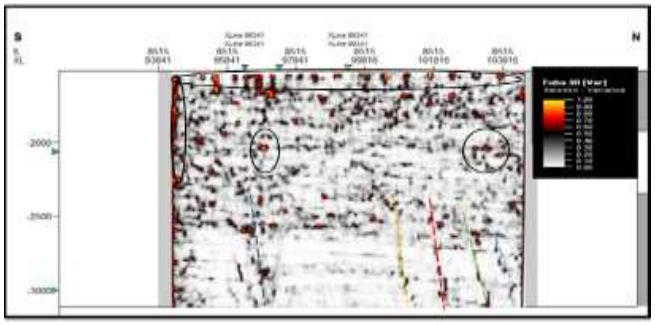

Figure 10. Variance Edge Inline 8515 Enhancing Faults and Indicating Potential Hydrocarbon Traps in Fuba Field.

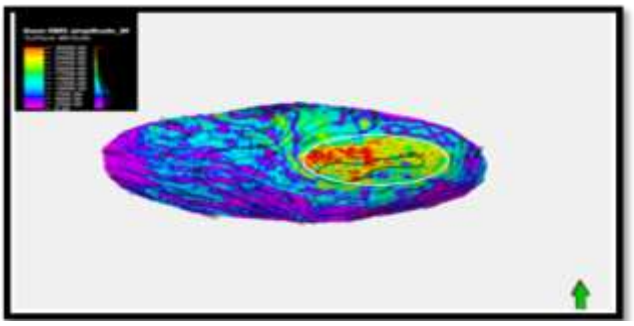

Figure 11. RMS Amplitude Map of Reservoir Surface M Showing High-Amplitude Zones Indicating Hydrocarbon Presence in Fuba Field.

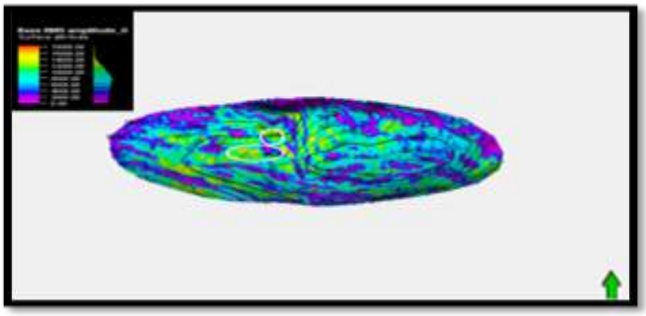

Figure 12. RMS Amplitude Map of Reservoir Surface O Showing High-Amplitude Zones Indicating the Presence of Hydrocarbon.

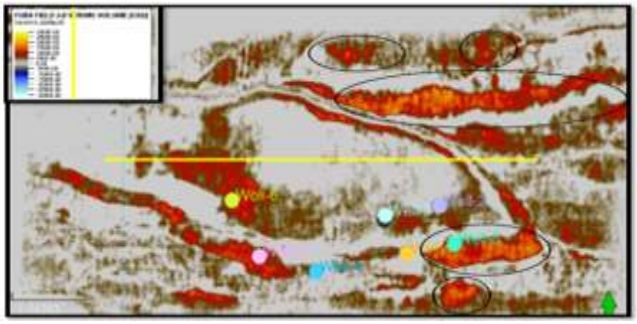

Figure 13. Spectral Decomposition at 35 Hz Showing Low-Frequency, High-Amplitude Hydrocarbon Zones.

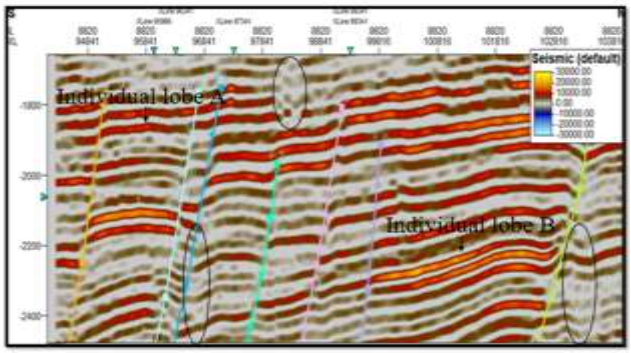

Figure 14. The General Spectral Decomposition at a Frequency of 35Hz Indicating Unconformity, the Presence of Lobes and Small Scale Faults in the Field

4.3. Seismic Attributes

Seismic attributes such as variance edge and Root Mean Square (RMS) amplitude and spectra were generated in Petrel software interface to investigate potential structural and stratigraphic controls within the study area.

Figure 10 shows the computed variance attributes of the seismic section. The variance values range from 0.0 to 1.0. Values of variance equal to 1 represent discontinuities while a continuous seismic event is represented by the value of 0. The high values are denoted with red to yellow colorations.

On the variance map, the areas dotted with blue, green, orange and pink colored lines signify values that correspond to the location of the discontinuity. The discontinuities may be interpreted as faults and boundaries as shown by the lines drawn on the variance attribute map (Law and Chung, 2006). The variance edge enhanced the faults or sedimentological bodies within the seismic data volume. Furthermore, several bright spots are also delineated (in black circles and black ovals) which indicate high reflectivity sediments compared to their surroundings. These bright spots are an indication that a potential hydrocarbon trap might exist in the area. The darkest regions in the seismic section, which make vertical strips, may be interpreted as faults or fractures. The zones with low variance values are due to similar seismic traces. Areas with red patches represent lineaments/discontinuities while grey areas represent the structural framework of the field.

The RMS amplitude was generated for the studied reservoir surfaces (reservoir surfaces M and O). The result of the RMS amplitude analysis is presented in Table 1 while Figures 11 and 12 show the RMS amplitude maps. The RMS amplitude values range from 0 (purple) to 13,000 (red) in reservoir M and from 0 (purple) to 9,000 (red) in horizon O. The red-yellowish colour represents hydrocarbon sands. Some of these hydrocarbon sands were not detected in the original seismic section. The observed changes may be due to changes in lithology or fluid content.

The RMS attribute is related to the variations in acoustic impedance. The higher the acoustic impedance values, the higher the RMS amplitude. The high values of RMS amplitudes may also be related to high porous sands, which are potential hydrocarbon reservoirs. RMS amplitude is similar to reflection strength and it is used in seismic exploration for delineating bright spots and amplitude anomalies (Fozoa, et al, 2018; Opara, and Osaki, 2018). The RMS amplitude is used for identifying coarser-grained facies, compaction related effects, and unconformities. The high values of RMS amplitudes circled (in white circles) in the maps are interpreted as high porosity lithologies, such as porous sands. These high RMS amplitude segments are potential high quality hydrocarbon reservoirs.

The high amplitude (in white circles) in the seismic data conforms to the structures and confirm the presence of hydrocarbon (Ajisafe, and Ako, 2013). The high amplitude ranges from light blue to yellow and red coloration. Root mean square amplitude is used as a good indicator of the presence of hydrocarbon in seismic data.

Table 1. RMS Amplitude Values for the Reservoir Surfaces

Reservoir	Range of RMS Amplitude Values
Reservoir-M	0 – 13,000
Reservoir _O	0 – 9,000

4.4. Spectral Decomposition

The general spectral decomposition was done at frequencies between 12Hz and 35Hz for the seismic. Figure 13 is the seismic volume obtained for the general spectral decomposition. Figure 13 illustrates Red-Green-Blue blend of the higher resolution of the frequency of 35Hz. The RGB colour blend effect gives a better understanding of the reservoirs geology. The colour blend is spectral balancing which recompense for wavelet and energy loss. The figure showed a complex meandering system and other less winding channels which are discontinuous and difficult to resolve on the seismic. The RGB colour blending slices revealed more hidden structures compared with what is observed in the time structural map. In this figure, the areas in red color indicate areas of low frequency and high amplitude associated with known hydrocarbon zones and when one colour is dominating, it showed that the frequency is dominating at that point. It revealed the geometry of the channels and other fewer sinusoidal channels. The channels are displayed with bright colouration which contains multiple frequencies as observed within the low frequency and high amplitude (indicated in black circles in Figure 13). At the north-eastern to the south-eastern part and south- western directions, there is high amplitude, an indication of hydrocarbon/gas effect. The acoustic impedance within the gas-bearing sand is lower compared to the surrounding shale (Naseer, and Asim, 2017). These are likely traps for hydrocarbon accumulation which are probable locations for drilling new wells of economic quantity; the portions of the field are where the thin beds are. This is very important in hydrocarbon exploration wells. The amplitude response which is dominated by blue colour is high frequency. At parts where there's a change in colour to brownish, it showed thickening up of the reflectors and greater contribution from the lower frequencies. There are colour changes in the channel system which could be indicative of changes in lithology.

4.5. Stratigraphic Contact

A major geologic feature was observed on the time-slice from the divergent pattern on the seismic section as we penetrate deeper, which is an unconformity (Figure 14). This represents a significant break in vertical velocity or breaks in deposition time or record on horizon (Neuendorf, et al, 2005). This type of unconformity is called angular unconformity. Angular unconformity is an unconformity between two groups of rocks whose bedding planes are not parallel or in which the older underlying rock dips at a different angle (usually steeper) than the younger, overlying strata. Its interpretation depends on the recognition of characteristic reflection geometries rather than on amplitude information. It shows that deposition of the sediments took place at different times. Some of the lobes are indicated in Figure 14 (individual lobes A and B).

As can be seen in the areas in black ovals in Figure 14, the results of spectral decomposition at frequencies between 12Hz and 35Hz indicates the presence of small-scale faults in the field.

5. Conclusion and Future Recommendations

A total of four sand bodies (L, M, N, and O) were identified and correlated across all seven wells in the field. Two horizons (M and O) were selected for the study. Structural analysis of the field revealed that reservoir M and O are anticlinal structures supported by two major bounding faults. Structural interpretation of seismic data revealed that the field is highly faulted with synthetic and antithetic faults which are in line with faults trends identified in the Niger Delta. All interpreted faults are normal synthetic and antithetic faults. A total of thirty-six faults were interpreted across the entire seismic data. Of the 36 interpreted faults, only F1 (synthetic fault) and F4 (antithetic fault) faults are regional, running from the top to bottom across the field. Hence, these faults play significant roles in trap formation at the upper, middle and lower sections of the field. Fault and horizon interpretation revealed that closures found on M and O reservoirs are collapsed crestal structures bounded by the two major faults. The depth structure maps reveal that the reservoirs are anticlinal and fault supported. Reservoirs are found at a shallower depth from 10937 to 10997 ft and at a deeper depth ranging from 11681 to 11871 ft. The synthetic and antithetic faults act as good traps for the hydrocarbon accumulation in the study area. The variance edge revealed the subtle structures and faults in the seismic section. The RMS amplitude values range from 0 to 13,000 in reservoir M and from 0 to 9,000 in horizon O. The high values of RMS amplitudes in the maps are interpreted as high porosity lithologies, such as porous sands. These high RMS amplitude segments are potential high quality hydrocarbon reservoirs.

The results of spectral decomposition indicate the following: (a) areas of low frequency and high amplitude associated with known hydrocarbon zones. (b) The presence of small-scale faults, channels, lobes and angular unconformity in the field. The result showed the validity of the technique and can also be used to propose a new drilling site. The seismic attribute analysis in this study has helped in increasing the understanding of the delineated reservoirs and geological structures in the study area towards a better delineation of hydrocarbon potential and improved reservoir characterization. Furthermore, it has been demonstrated that seismic attributes are complementary to the information derived through traditional methods of seismic interpretation. In reservoirs, hydrocarbons were encountered by all seven wells drilled in the field. The following are some future suggestions (i) Studies should be done on the field's evidence of subsidence induced by hydrocarbon-production (ii) Fault seal analysis should be carried out to confirm that the suspected trapping faults are not leaking in which case they serve as conduits for hydrocarbon migrations rather than lateral barriers to hydrocarbon escape. (iii) Studies should be done on the mapping of thin sandstone reservoirs in the study area. (iv) Studies should be done using geomechanical modeling to quantify the stress changes and strains in a synthetic model for the formations in and around the depleting reservoirs. (v) Studies should be done on the impact of structural setting on hydrocarbon trapping mechanism of the study area using seismic attributes analysis.

Declaration

Source of Funding

This study did not receive any grant from funding agencies in the public, commercial, or not-for-profit sectors.

Competing Interests Statement

The author declares no competing financial, professional, or personal interest.

Consent for Publication

The author declares that she consented to the publication of this study.

Author's Contribution

The author declares that she carried out the study.

Informed Consent

Not applicable.

Availability of Data and Material

The data and material used for this study was made available by Shell Petroleum Development Company of Nigeria (SPDC), Port Harcourt Nigeria.

Institutional Review Board Statement

Not applicable.

Ethical Approval

Not applicable.

Acknowledgements

The author is grateful to Shell Petroleum Development Company of Nigeria (SPDC), Port Harcourt Nigeria for the release of the academic data for the purpose of this study.

Declaration of Artificial Intelligence

The author declares that she did not use artificial intelligence during the course of this study.

References

[1] Abraham-A, R.M., & Taioli, F. (2018). Redefining fluids relative permeability for reservoir sands, Osland Oil and Gas Field, Offshore Niger Delta Nigeria. Journal of African Earth Science, 142: 218–225.

[2] Abimbola, L.A., & Emujakporue, G. (2020). 3D seismic structural interpretation of Riche Field, Onshore Niger Delta. International Journal of Scientific Research and Engineering Development, 3(1), 300-312.

[3] Majid, K., Shahid, N., Munawar, S., & Muhammad, H. (2016). Interpreting seismic profiles in terms of structure and stratigraphy with implications for hydrocarbons accumulation, an example from lower Indus Basin Pakistan. Journal of Geology and Geophysics, 5(5): 257.

[4] Adebayo, S.S., Agbalagba, E.O., Korode, A.I., Fagbemigun, T.S., Oyanameh, O.E., & Osisanya, O.W. (2021). 3-D seismic structural interpretation of High Field Offshore Western Niger Delta. Journal of Applied Science and Environmental Management, 26(8): 1361–1369.

[5] Coffeen, J.A. (1984). Seismic exploration fundamentals. PennWell Publication Company.

[6] Doust, H., & Omatsola, E. (1990). Niger Delta margin basins. AAPG Memoir, 48: 239–248.

[7] Emujakporue, G.O., & Ngwueke, M.I. (2013). Structural interpretation of seismic data from an XY Field, Onshore Niger Delta, Nigeria. Journal of Applied Sciences and Environmental Management, 17(1): 153–158.

[8] Folami, T.O., Ayuk, M.A., & Adesida, A. (2008). Identification of hydrocarbon reservoirs using seismic attributes and geocellular modelling: A case study from "Tyke" Field, Niger Delta, Nigeria. Association of Petroleum Geologists Bulletin: 30–32.

[9] Aigbedion, I., & Hafiz, A.I. (2016). Evaluation of hydrocarbon prospect of Fareed Field. International Journal of Geography, Environment and Earth Science, 7(4): 1–8.

[10] Omoja, U.C., & Obiekezie, T.N. (2019). Application of 3D seismic attribute analyses for hydrocarbon prospectivity in Uzot-Field, Onshore Niger Delta Basin, Nigeria. International J. of Geophysics, 2019(2): 1–11.

[11] Whiteman, A. (1982). Nigeria: Its petroleum ecology resources and potential. Graham and Trotman, London.

[12] Adegoke, O.S., Oyebamiji, A.S., Edet, J.J., Osterloff, P.L., & Ulu, O.K. (2017). Cenozoic foraminifera and calcareous nannofossil biostratigraphy of the Niger Delta. Elsevier, Cathleen Sether, United States.

[13] Short, K.C., & Stable, A.J. (1967). Outline of geology of Niger Delta. Bulletin of American Association of Petroleum Geologists, 51(5): 761–779.

[14] Horsfall, O.I., Uko, E.D., Tamunoberetonari, I., & Omubo-Pepple, V.B. (2017). Rock-physics and seismic-inversion based reservoir characterization of AKOS FIELD, Coastal Swamp Depobelt, Niger Delta, Nigeria. IOSR Journal of Applied Geology and Geophysics, 5(4): 59–67.

[15] Ochoma, U. (2023). Application of 3-D seismic attributes analysis for hydrocarbon prospectivity in Onshore Fuba Field, Niger Delta, Nigeria. Asian Journal of Basic Science and Research, 5(2): 83–96.

[16] Ochoma, U., Tamunobereton-ari, I., Amakiri, A.R.C., Sigalo, F.B., Horsfall, O.I., & Davies, O.A. (2023). Identification of hydrocarbon trapping mechanisms in Fuba Field, Onshore Niger Delta, Nigeria. Asian Journal of Applied Science and Technology (AJAST), 7(2): 23–32.

[17] Aizebeokhai, A.P., & Olayinka, I. (2011). Structural and stratigraphic mapping of EMI Field, Offshore Niger Delta. Journal of Geology and Mining, 3(2): 25–38.

[18] Hafiz, A., Aigbedion, I., Iyoha, A., Aigbedion, E.O., Ataman, J.O., Salufu, S., Ozegin, K.O., & Shaibu, I. (2024). Structural styles and hydrocarbon trapping mechanisms onshore and offshore, Niger Delta. International Journal of Science for Global Sustainability, 10(1): 123–131.

[19] Ameloko, A.A., & Owoseni, A.M. (2015). Hydrocarbon reservoir evaluation of X-field, Niger Delta using seismic and petrophysical data. International Journal of Innovation and Scientific Research, 15(1): 193–201.

[20] Sulistiyono, S., Sendjaja, Y.A., Abdurrokhim, A., & Adhiperdana, B.G. (2025). Geohistory model and structural style for hydrocarbon trapping mechanism in Kendal Sub-basin, North Central Java, Indonesia. Iraqi Geological Journal, 58(2A): 165–183.

[21] Yousif, H., Huang, X., & Zhang, G. (2025). Role of faulting in salt deformation and hydrocarbon trapping in the Missan Oilfields, Southeastern Iraq. Geosciences, 15(11): 439–462.

[22] Pigott, J.D., Kang, M.I.H., & Han, H.C. (2013). First order seismic attributes for clastic seismic facies interpretation: Examples from the East China Sea. Journal of Asian Earth Science, 66: 34–54.

[23] Cohen, L. (1989). Time-frequency distributions-a review. Proceedings of the IEEE, Pages 941–981.

[24] Law, W.K., & Chung, A.S.C. (2006). Minimal weighted local variance as edge detector for active contour models. In Narayanan, P.J. (Ed.), LNCS 3851, Pages 622–632.

[25] Fozao, K.F., Fotso, L., Djieto-Lordon, A., & Mbeleg, M. (2018). Hydrocarbon inventory of the eastern part of the Rio Del Rey Basin using seismic attributes. Journal of Petroleum Exploration and Production Technology, 8(1): 655–665.

[26] Opara, A.I., & Osaki, L.J. (2018). 3-D seismic attribute analysis for enhanced prospect definition of "Opu Field", Coastal Swamp Depo Belt Niger Delta, Nigeria. Journal of Applied Science, 18(2): 86–102.

[27] Ajisafe, Y.C., & Ako, B.D. (2013). 3-D seismic attributes for reservoir characterization of 'Y' Field, Niger Delta, Nigeria. IOSR Journal of Applied Geology and Geophysics, 1(2): 23–31.

[28] Naseer, M.T., & Asim, S.N. (2017). Detection of Cretaceous incised valley shale for resource play, Miano Gas Field, SW Pakistan: Spectral decomposition using continuous wavelet transform. Journal of Asian Earth Science, 147(2): 358–377.

[29] Neuendorf, K.K.E., Mehl, J.P., & Jackson, J.A. (2005). Glossary of geology. 5th edn. American Geological Institute, Alexandria, Virginia, Pages 779.